Progress In Electromagnetics Research, Vol. 131, 441–455, 2012

FULL-WAVELENGTH DIPOLE ANTENNA ON A GaAs MEMBRANE COVERED BY A FREQUENCY SELECTIVE SURFACE FOR A TERAHERTZ PHOTOMIXER

T. K. Nguyen[1], T. A. Ho[1], I. Park[1, *], and H. Han[2]

[1]School of Electrical and Computer Engineering, Ajou University, 5 Woncheon-dong, Youngtong-gu, Suwon 443-749, Korea

[2]Department of Electrical and Computer Engineering, POSTECH, San 31 Hoyja-dong, Nam-gu, Pohang 790-784, Korea

Abstract—An antenna consisting of a full-wavelength dipole on a GaAs membrane covered by a frequency selective surface is proposed for improved output power from photomixers used as terahertz (THz) sources. The antenna structure reduces the vertical dimension of a typical photomixer antenna using a substrate lens while still exhibiting high total efficiency and high directivity. The resulting antenna after optimization produced an input resistance of 3870 Ω and a radiation efficiency of 60%, corresponding to a total efficiency, i.e., the efficiency of the antenna in THz wave radiation, of approximately 48.3% and a maximum directivity of 20.2 dBi at the resonance frequency of 1.03 THz. The proposed antenna is expected to be a promising alternative THz photomixer design.

1. INTRODUCTION

The terahertz (THz) frequency region, which is loosely defined as 0.1–10 THz, has long been known as "the THz gap" although THz science and technology have made significant progress in the past decades [1–4]. The lack of suitable and efficient signal sources limits applications to a number of areas that demand highly reliable performance, ranging from molecular spectroscopy to astronomy, environmental monitoring, bio-imaging, and security screening [5–9]. A room-temperature-operation continuous wave (CW) THz source would greatly benefit many of the aforementioned THz applications, and especially narrow-bandwidth high-resolution spectroscopy and

Received 21 August 2012, Accepted 31 August 2012, Scheduled 17 September 2012

* Corresponding author: Ikmo Park (ipark@ajou.ac.kr).

imaging [10, 11]. Quantum cascade lasers (QCLs) and photomixers are promising semiconductor-based CW terahertz sources; however, QCLs typically require cryogenic cooling, particularly at the lower THz range [12, 13]. Owing to their operability at room temperature, compactness, and widely tunable frequency range, photomixers have proven more promising as CW THz sources [14–18]. The efficiency of such devices is determined by the internal efficiency of the semiconductor material used and the efficiency of the antenna in THz wave radiation [19]. Recently, a novel approach which greatly enhanced CW THz emission using nano-electrodes in a photoconductive photomixer has been successfully implemented [20]. This approach significantly overcomes one of the two main drawbacks causing low output power of THz photomixer designs, the low conversion efficiency of the photomixer from the incident laser to the THz photocurrent. Another drawback is the low total efficiency of the antenna from the THz photocurrent to the THz radiated wave which requires particular antenna designs. Antenna efficiency is derived as a product of the impedance matching and radiation efficiencies, both of which are considerable concerns in a THz antenna design [21]. Generally speaking, the impedance of the antenna is much lower than the output impedance of the photomixer, typically greater than $10\,\mathrm{k}\Omega$ when photomixing two incident CW lasers, even at antenna resonance. This severe impedance mismatch degrades the THz output power of a THz photomixer design. The radiation efficiency is also particularly important due to the resonance effects of the antenna structure and the reduced conductivity of the metal at THz frequencies. Therefore, an antenna design with high input resistance and high radiation efficiency would yield a high total efficiency and significantly improve the conversion efficiency of the THz photocurrent into the THz wave [22].

Besides having high total efficiency, a THz photomixer antenna must be highly directional in order to serve as either a photomixing emitter or detector — both of which are key components of CW THz systems. To increase the directivity of a THz photomixer antenna, large area emitters using an array of photomixers driven coherently by the same pair of lasers have shown promise [23]. However, this configuration requires higher illumination power from the two CW laser sources. A lens substrate is an alternate approach since it can eliminate the total internal reflection and increase the directivity of the radiation pattern through beam focusing [24]. However, dielectric lenses made of high permittivity material such as silicon (Si, $\varepsilon_r = 11.7$) or gallium arsenide (GaAs, $\varepsilon_r = 12.9$) cause significant reduction of the antenna input resistance. Recently, a configuration with the lens substrate

not in contact with the radiating element has been proposed, thus avoiding the input resistance reduction of the antenna while exhibiting high directivity characteristics [25]. Nevertheless, to obtain similar directivity patterns the lens design are considered as much longer wavelength involved in comparison with the FSS design. For instance to achieve an approximate 20 dBi directivity, a total vertical dimension of a typical lens design is about few wavelength while that of an FSS design with only approximately half wavelength at the same resonance frequency.

In this paper, we propose a THz photomixer antenna covered by a frequency selective surface (FSS) to reduce the vertical dimension while still exhibiting both high total efficiency and high directivity characteristics. The paper is organized as follows. First, we describe the actual prototype of the antenna including the geometry of the GaAs membrane structure. A full-wave electromagnetic simulator, Microwave Studio by CST [26], is then used for modeling the antenna and optimization of the antenna directivity and total efficiency at the desired frequency. In this optimization, the size of the cavity in GaAs substrate, the number of circular holes in FSS, and the thickness of a dielectric layer supporting the FSS are varied. For each of those parameters, we identify trade-offs between the obtained directivity and total efficiency. The final design and optimized results are presented in the last section.

2. DESCRIPTION AND MODELING OF THE STRUCTURE

Figure 1 shows the geometry of the proposed antenna with the front view of the whole structure and top views of the FSS, the GaAs ($\varepsilon_{r1} = 12.9$) membrane and the ground plane layer. The FSS and the ground plane, whose distance apart, H, is approximately a half-wavelength at the resonance frequency, form a resonator. The ground plane acts as a perfect mirror, and the FSS acts as a partially reflective mirror. The FSS is a circular hole array whose unit cell has periodicity and radius of p and r, respectively. The FSS is supported by a quartz substrate placed on the top and has the same size as the GaAs membrane structure for easy alignment. The procedure used to form the GaAs membrane structure was detailed in our previous work [22, 25]. In this design, we used a full-wavelength dipole with a total length L_d of 120 µm and a width w_d of 3 µm as a radiator for simplification and to obtain high input resistance. Since the antenna radiates from the front side, a small circular hole is introduced at the ground center, yielding a back-excitation configuration. The

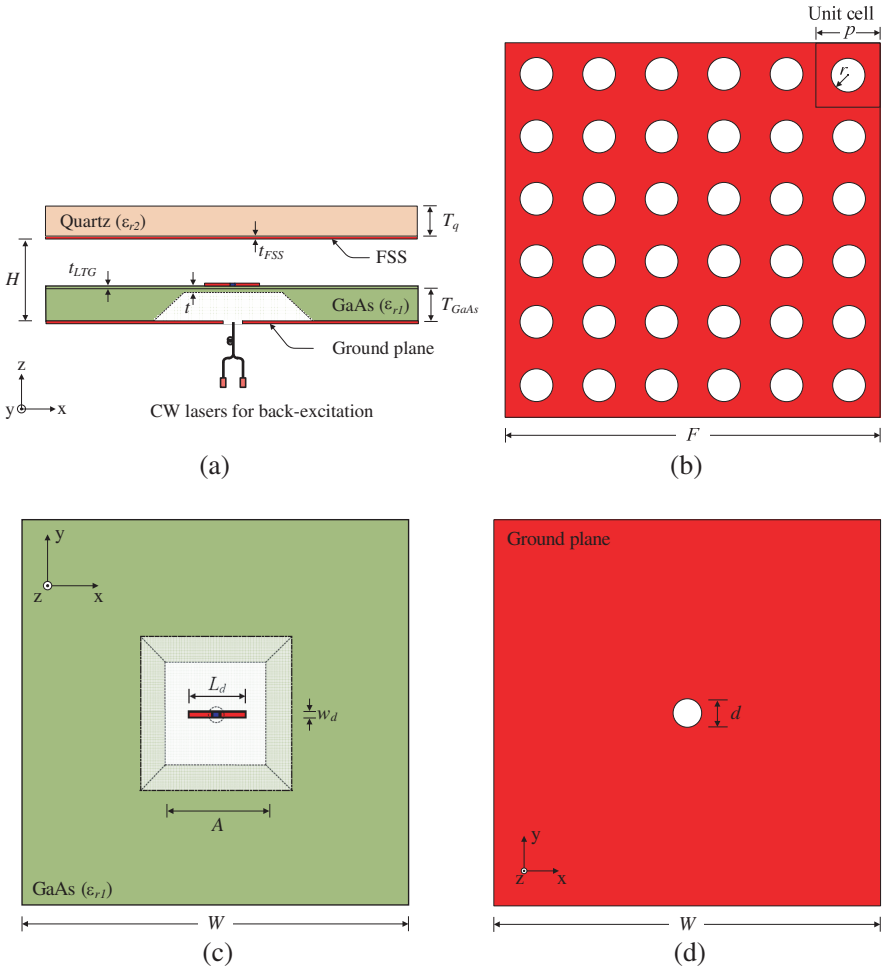

Figure 1. Antenna geometry with (a) front view, (b) top view of the FSS layer, (c) top view of the GaAs membrane substrate, and (d) top view of the ground plane.

FSS, dipole, and the ground plane were modeled with a titanium-gold (Ti-Au) thin film with a thickness of 0.35 μm and a conductivity of 1.6×10^7 S/m.

For purposes of studying the transmission characteristic, it is possible to assume that a unit cell consists of a half-wavelength resonator, a single circular hole supporting by quartz substrate, a thin membrane (thickness of t and suspended at distance T_{GaAs} above the ground plane), and a ground plane. Thus, the transmission

behavior and resonance frequency can be easily predicted by modeling a simplified unit cell excited by a plane wave. Three principle parameters, the distance H between the ground plane and the FSS, the periodicity p, and the hole radius r, were first studied to obtain the optimum propagation properties of the resonator. After optimization of the transmission, a full FSS structure was designed on top of the GaAs membrane. The input resistance, radiation efficiency and directivity of the antenna at resonance were studied and analyzed.

3. THZ PHOTOMIXER AND ANTENNA CHARACTERISTICS

In our design, the total efficiency and the directivity of the antenna are particularly important. The total efficiency in a THz antenna design is the product of the internal efficiency (or laser-to-electrical power-conversion efficiency) ε_{LE}, the radiation efficiency $\varepsilon_{\text{radiation}}$, and the impedance matching efficiency $\varepsilon_{\text{match}}$ [19] and can be expressed as:

$$\varepsilon_{\text{total}} = \varepsilon_{\text{LE}} \times \varepsilon_{\text{radiation}} \times \varepsilon_{\text{match}} \tag{1}$$

In this expression, the impedance-matching efficiency is calculated from

$$\varepsilon_{\text{match}} = 1 - \left| \frac{Z_{\text{antenna}} - Z^*_{\text{photomixer}}}{Z_{\text{antenna}} + Z^*_{\text{photomixer}}} \right|^2 \tag{2}$$

where Z_{antenna} and $Z_{\text{photomixer}}$ are the impedance of the antenna and photomixer, respectively, and * denotes the complex conjugate. A photomixer impedance of $10\,\text{k}\Omega$ is assumed in the impedance-matching efficiency calculation. The impedance matching and radiation efficiencies for a given antenna can be obtained using an electromagnetic simulator. The laser-to-electrical power-conversion efficiency is very difficult to estimate accurately, and typically depends on factors such as the photoconductive material, excitation power, and bias conditions. This efficiency is very small, resulting in extremely low total photomixer efficiency. Clearly, improving the laser-to-electrical power-conversion efficiency, matching efficiency and radiation efficiency of the antenna would significantly improve the total efficiency of a THz photomixer design. In this paper, we only consider the matching efficiency and radiation efficiency of the antenna in our calculations since the laser-to-electrical power-conversion efficiency is not highly dependent on the antenna design. The directivity of the antenna was checked from the radiation patterns at a single direction of $\theta = 0°$. In each parameter study and analysis, performance evaluations and trade-offs of the total efficiency and antenna directivity have been carefully considered.

3.1. Effect of the Size of Cavity in a GaAs Substrate

Figure 2 shows the variation of the antenna performance in terms of the radiation efficiency, input resistance, and directivity with respect to changes in the cavity size A. The substrate geometry was initially chosen with the bulk substrate size W of 5000 µm, substrate thickness T_{GaAs} of 10 µm, and membrane thickness t of 3 µm. For the FSS, the circular hole array had a periodicity p of 86 µm and a radius r of 32 µm, supported by a quartz substrate ($\varepsilon_{r2} = 4$) having a thickness T_q of 25 µm. The FSS and the ground plane were distance H apart of 135 µm, which is approximately a half wavelength at the frequency of directivity enhancement, i.e., 1.03 THz. The radiation efficiency and input resistance of the antenna were almost constant [Figure 2(a)]. We also observed that the resonance frequency where the peak input resistance occurred was constant. This indicates that the total efficiency is stable with the changes of the cavity size. However, the directivity of the antenna behaved differently [Figure 2(b)]. As the cavity size increased from 500 to 2000 µm, the directivity gradually increased from 16.2 dBi to more than 20 dBi, representing an approximately 4-dB improvement. The directivity then showed a saturation with a minimal change as the cavity size was further increased. Therefore, the expected high directivity was not obtained for small cavity sizes but rather for larger cavities.

The current distributions induced on the circular hole array for cavity sizes of $A = 1000$ µm and $A = 2000$ µm, as calculated at the resonance frequency, are depicted in Figure 3. This figure shows that

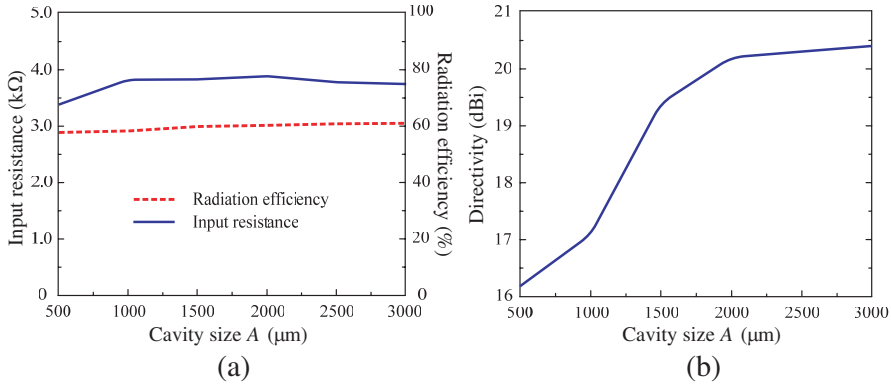

Figure 2. (a) Input resistance and radiation efficiency and (b) directivity of the antenna with respect to the changes of the cavity size (A).

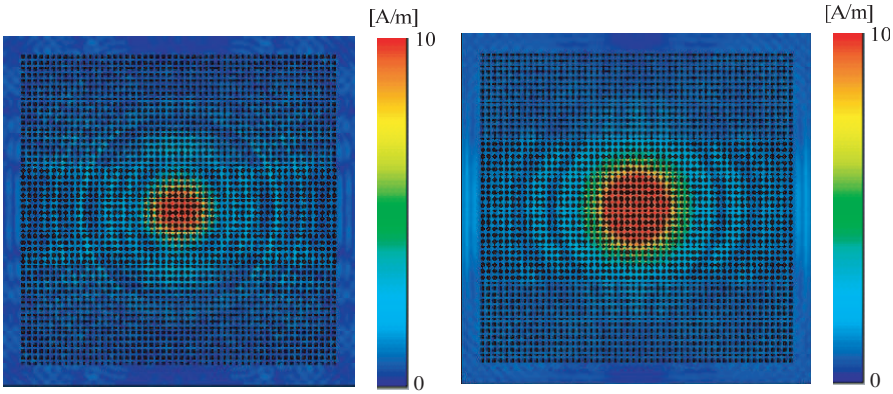

Figure 3. Current distribution induced on the FSS for two different cavity sizes; (a) $A = 1000\,\mu m$ and (b) $A = 2000\,\mu m$.

only circular holes at the center portion of the array are excited and take part into the transmission enhancement and not the entire array. This effective area is approximately equal to the cavity size. The phase shift of the electromagnetic wave in each return can only be superposed in phase within this region to satisfy the resonance condition, that is, a half-wavelength distance between the ground plane and the FSS layer. Larger cavity sizes more effectively illuminate the holes for enhanced transmission, i.e., improved antenna directivity. This observation confirms that the cavity size plays an important role in controlling the maximum directivity. In the optimized design, we chose a cavity size of $A = 2000\,\mu m$ for maximum directivity.

3.2. Effect of the Number of Holes in a Array

We performed a study on how the antenna performance responds to changes in the number of holes in the array for cavity sizes of $A = 1000\,\mu m$, $1500\,\mu m$, and $2000\,\mu m$. The input resistance, radiation efficiency, and directivity of the antenna were evaluated and plotted in Figures 4(a)–(c), respectively. The input resistance and radiation efficiency of the antenna were not significantly affected by the number of holes. There was only an approximate 4% variation of input resistance and 2% variation of radiation efficiency as the periodic hole array increased from 8×8 to 28×28 in size. Therefore, the total efficiency of the antenna was not significantly changed owing to the number of holes in the FSS regardless of cavity size. The directivity of the antenna, however, showed distinctly different behavior. As

the cavity size approached 1000 µm, we observed an almost constant maximum directivity regardless of number of holes. Here, the cavity size is too small and accordingly the number of effective holes is not sufficient to have the required effect on directivity. However, a transition was obvious for larger cavities, i.e., $A = 1500\,\mu m$ and $A = 2000\,\mu m$. The directivity increased about 1.8 dB and 2.3 dB as the number of holes increased from 8×8 to 16×16 for $A = 1500\,\mu m$ and $A = 2000\,\mu m$, respectively. Saturation occurred as the number of array holes was further increased beyond 16×16.

Figure 5 shows the radiation patterns of the antenna with differing numbers of holes in the array for a cavity size of $A = 2000\,\mu m$. Significant improvement in the main lobe and the side lobe was obtained as the number of holes in the array increased from 8×8 holes

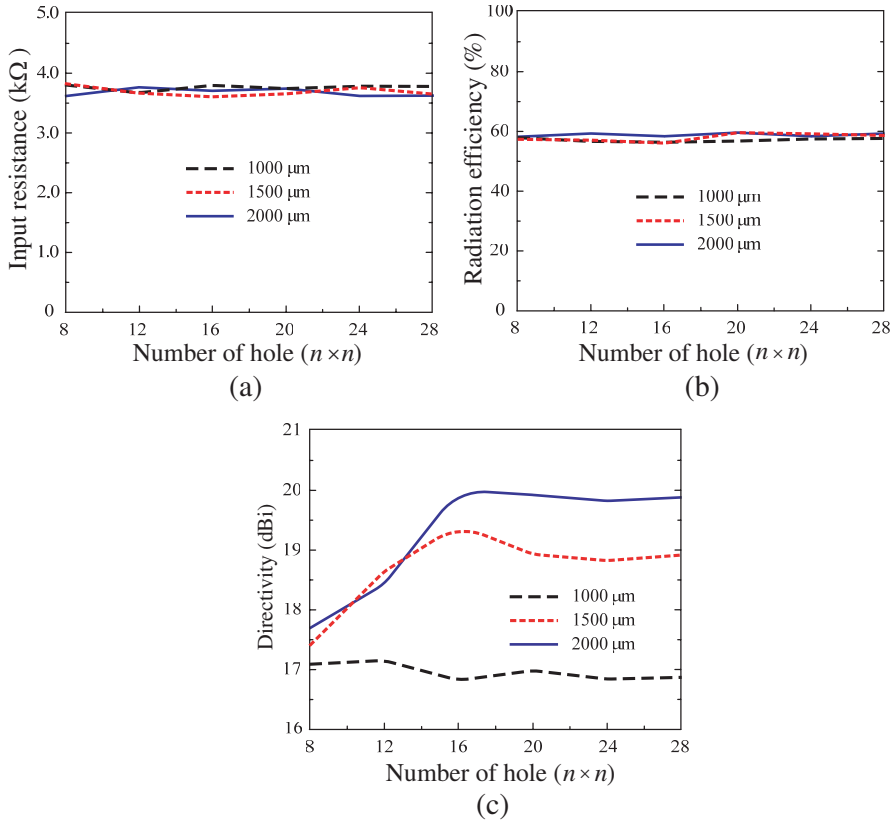

Figure 4. (a) Input resistance, (b) radiation efficiency, and (c) directivity of the antenna with respect to the changes of the number of holes in the FSS for different cavity sizes (A).

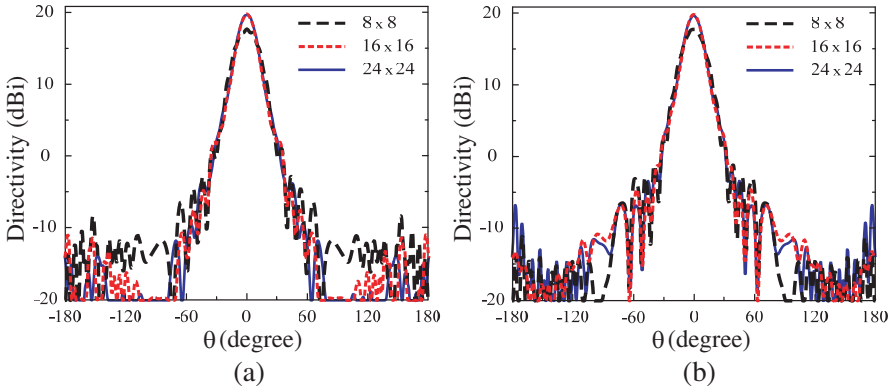

Figure 5. Radiation patterns in (a) the x-z plane and (b) the y-z plane of the antenna with different numbers of holes in the array where $A = 2000\,\mu\text{m}$.

to 16×16 holes. The main lobes became narrower and the side lobes reduced both in the x-z and y-z planes. Maximum directivity increased approximately 2.3 dB as the array size increased from 8×8 holes to 16×16 holes. The patterns, however, remained essentially constant as the array increased from 16×16 holes to 24×24 holes. These observations again verify that only a portion of array, corresponding to the cavity size region, contributes to the transmission enhancement of the proposed antenna. In addition, transmission enhancement can occur with a finite array containing a sufficient number of elementary cells. In the proposed design, the FSS of 16×16 periodic holes is found to be a minimum size to achieve both the enhanced transmission property and the improved antenna directivity.

3.3. Effect of the Dielectric Quartz Substrate Supporting the Hole Array

The circular hole array is supported by a quartz substrate with a dielectric constant of $\varepsilon_{r2} = 4$ and a thickness of T_q. Figure 6 shows the resonance frequency response versus the thickness T_q when two different quartz substrate positions were examined, i.e., on the top and at the bottom of the FSS. Other design parameters except the quartz thickness are the same as in Subsection 3.1. When the quartz layer was positioned on the top of the hole array, the resonance frequency exhibited a very slight variation as the quartz thickness increased. However, the resonance frequency gradually decreased with increasing quartz thickness when the layer was positioned at the bottom of the hole array. This behavior can be explained by the increased effective

index of the resonator medium bounded by the ground plane and the metal hole array. Consequently, the resonance length of the resonator, i.e., the distance between the ground and the FSS, has to be increased to compensate for this reduction of the resonance frequency. In addition, the electromagnetic waves are reflected or trapped in the dielectric substrate prior to reaching the hole array. Therefore, the quartz dielectric layer is better placed at the top of the FSS in order to support the hole array and preclude the aforementioned problems.

Figure 7 shows that the quartz thickness has considerable effect on the antenna performance. The quartz substrate was positioned at the top of the FSS and its thickness was varied from 0 to 50 μm. As the quartz thickness increased, the radiation efficiency showed a peak while the matching efficiency, corresponding to the input resistance, showed a dip at $T_q = 25\,\mu\text{m}$ ($\sim 0.1\lambda_0$). This value coincides closely with the cut-off thickness of the TE_0 mode in the quartz substrate, thus affording the maximum radiation efficiency [27]. The total efficiency consequently showed a maximum at this value of T_q. However, the maximum directivity of the antenna occurred with a thinner quartz substrate, i.e., $T_q = 15\,\mu\text{m}$. When T_q increased from 15 μm to 25 μm, there was an increase of approximately 16% in the radiation efficiency, or an absolute increment of 6.6% from 41.7% to 48.3%. At the same time, the directivity of the antenna decreased by only 3% or 0.6 dB from 20.8 to 20.2 dBi. From these data, we concluded that the optimum thickness of the quartz substrate was $T_q = 25\,\mu\text{m}$.

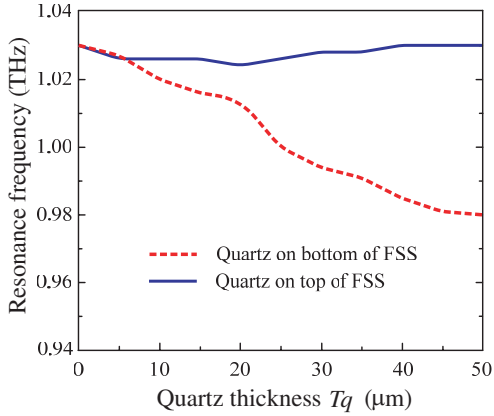

Figure 6. Resonance frequency with respect to the position of the quartz substrate.

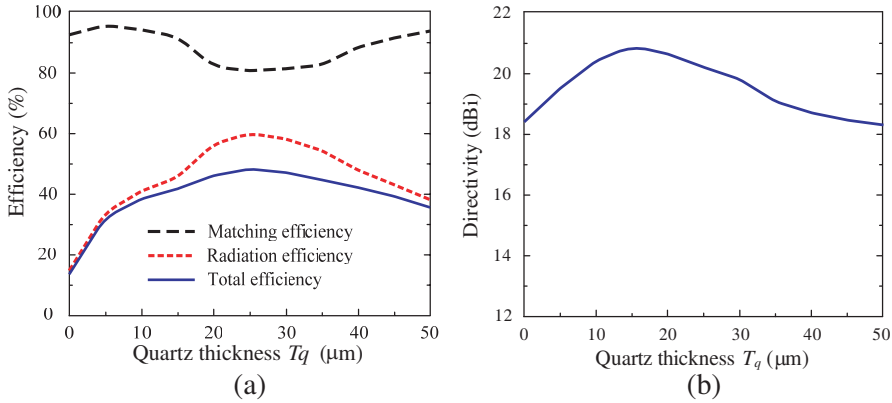

Figure 7. (a) Efficiency and (b) directivity of the antenna with respect to the quartz substrate thickness variation.

Table 1. Design parameters for maximum total efficiency and directivity at 1.03 THz of the proposed antenna.

Parameter	Dimension (μm)	Parameter	Dimension (μm)
W	5000	F	5000
A	2000	T_q	25
T_{GaAs}	10	p	86
t_{LTG}	1	r	32
t	3	t_{FSS}	0.35
L_d	120	H	135
w_d	3	d	20

4. FINAL DESIGN AND SIMULATED RESULTS

Design parameters for optimum antenna performance are summarized in Table 1. Figure 8(a) plots the input resistance and radiation efficiency versus frequency of the proposed antenna. The antenna produced an input resistance of 3870 Ω, or about 80.5% matching efficiency, and a radiation efficiency of 60%, corresponding to an approximate total efficiency of 48.3% at the resonance frequency of 1.03 THz. The directivity of the proposed antenna versus frequency is plotted in Figure 8(b). We find a passband 3-dB directivity of about 5% for a maximum directivity of 20.2 dBi at the same resonance frequency. The radiation patterns in the x-z and y-z plane plotted at the resonance frequency are shown in Figure 8(c), exhibiting

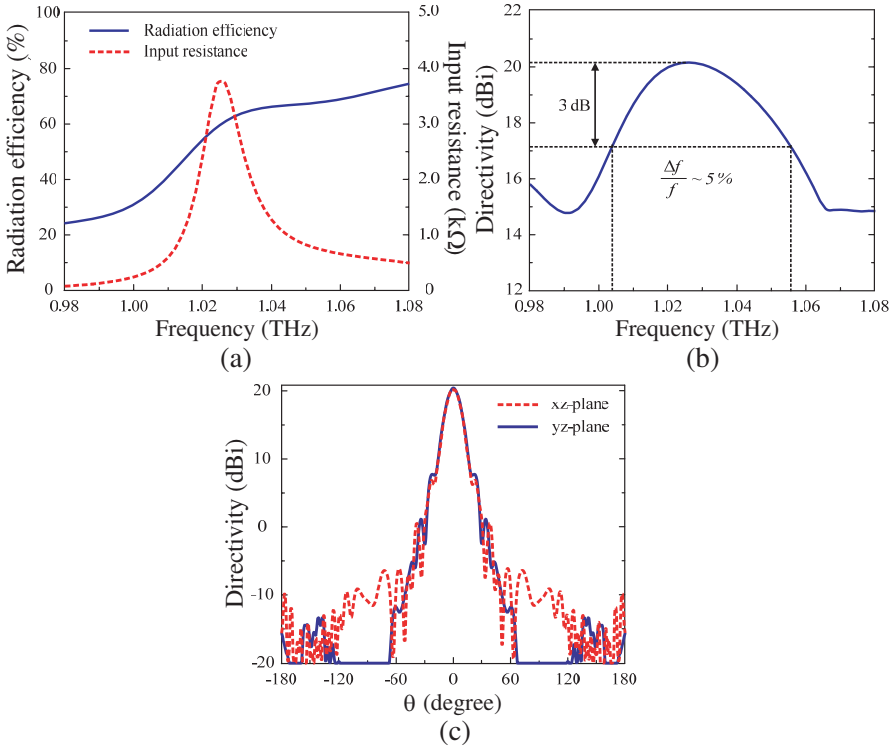

Figure 8. Simulated results of the optimized antenna (a) input resistance and radiation efficiency, (b) directivity, and (c) radiation patterns at the resonance frequency of 1.03 THz.

symmetric characteristics. The half-power-beamwidths (HPBWs), side-lobe-levels (SLLs), and front-to-back (F/B) ratio of the optimized antenna were 16.7°, −13.3 dB, and 29.8 dB in the x-z plane and 16.3°, −12.6 dB, and 36.1 dB in the y-z plane.

5. CONCLUSIONS

We designed a compact antenna structure for a THz photomixer that produced both high total efficiency and high directivity. The antenna consisted of a full-wavelength dipole printed on a GaAs membrane structure for increased total efficiency, and an FSS structure for improved directivity. The effects of the cavity size in the GaAs membrane, the number of holes in the FSS, and the thickness of the quartz substrate supporting the hole array were characterized

and optimized. Trade-offs between the obtained directivity and total efficiency were found in each parameter study, verifying the importance of the antenna geometry in performance optimization. The resulting antenna after optimization produced an input resistance of 3870 Ω and a radiation efficiency of 60%, corresponding to approximately 48.3% total efficiency, (excluding the laser-to-electrical power-conversion efficiency), and a maximum directivity of 20.2 dBi at the resonance frequency of 1.03 THz. Further work with multiple stacked FSS could be carried out to enhance the directivity with particular consideration given to the total efficiency of the antenna. The proposed antenna is expected to be a good alternative for a highly efficient THz photomixer design.

ACKNOWLEDGMENT

This work was supported by a National Research Foundation of Korea grant funded by the Korean Government (grant code: 2009-0083512).

REFERENCES

1. Zhong, S., Y. Shen, H. Shen, and Y. Huang, "FDTD study of a novel terahertz emitter with electrical field enhancement using surface plasmon resonance," *PIERS Online*, Vol. 6, No. 2, 153–156, 2010.
2. Lucyszyn, S. and Y. Zhou, "Engineering approach to modeling frequency dispersion within normal metals at room temperature for THz applications," *Progress In Electromagnetics Research*, Vol. 101, 257–275, 2010.
3. Zhou, H., F. Ding, Y. Jin, and S. He, "Terahertz metamaterial modulators based on absorption," *Progress In Electromagnetics Research*, Vol. 119, 449–460, 2011.
4. Andres-Garcia, B., L. E. Garcia-Munoz, D. Segovia-Vargas, I. Camara-Mayorga, and R. Gusten, "Ultrawideband antenna excited by a photomixer for terahertz band," *Progress In Electromagnetics Research*, Vol. 114, 1–15, 2011.
5. Winnewisser, G., "Spectroscopy in the terahertz region," *Vibrat. Spectrosc.*, Vol. 8, 241–253, 1995.
6. Siegel, P. H., "Terahertz technology," *IEEE Trans. Microw. Theory Tech.*, Vol. 50, No. 3, 910–928, Mar. 2002.
7. Cai, M. and E. P. Li, "A novel terahertz sensing device comprising of a parabolic reflective surface and a bi-conical structure," *Progress In Electromagnetics Research*, Vol. 97, 61–73, 2009.

8. Hu, B. B. and M. C. Nuss, "Imaging with terahertz waves," *Opt. Lett.*, Vol. 20, No. 16, 1716–1718, Aug. 1995.
9. Shen, Y. C., T. Lo, P. F. Taday, B. E. Cole, W. R. Tribe, and M. C. Kemp, "Detection and identification of explosives using terahertz pulsed spectroscopic imaging," *Appl. Phys. Lett.*, Vol. 86, 241116, 2005.
10. Tonouchi, M., "Cutting-edge terahertz technology," *Nature Photon.*, Vol. 1, 97–105, 2007.
11. Williams, B. S., "Terahertz quantum-cascade lasers," *Nature Photon.*, Vol. 1, 517–525, Sep. 2007.
12. Maineult, W., P. Gellie, A. Andronico, P. Filloux, G. Leo, C. Sirtori, S. Barbieri, E. Peytavit, T. Akalin, J.-F. Lampin, H. E. Beere, and D. A. Ritchie, "Metal-metal terahertz quantum cascade laser with micro-transverse-electromagnetic-horn antenna," *Appl. Phys. Lett.*, Vol. 93, No. 18, 183508, 2008.
13. Kumar, S., Q. Hu, and J. L. Reno, "186 K operation of terahertz quantum-cascade lasers based on a diagonal design," *Appl. Phys. Lett.*, Vol. 94, 131105, 2009.
14. Preu, S., G. H. Döhler, S. Malzer, L. J. Wang, and A. C. Gossard, "Tunable, continuous-wave terahertz photomixer sources and applications," *J. Appl. Phys.*, Vol. 109, 061301, 2011.
15. Brown, E. R., "Advancements in photomixing and photoconductive switching for THz spectroscopy and imaging," *Proc. SPIE7938*, 793802, 2011.
16. Plínski, E. F., "Terahertz photomixer," *Technical Sciences*, Vol. 58, No. 4, 2010.
17. Gregory, I. S., W. R, Tribe, B. E. Cole, M. J. Evans, E. H. Linfield, A. G. Davies, and M. Missous, "Resonant dipole antennas for continuous-wave terahertz photomixers," *Appl. Phys. Lett.*, Vol. 85, 1622–1624, 2004.
18. Saeedkia, D. and S. Safavi-Naeini, "Terahertz photonics: Optoelectronic technique for generation and detection of terahertz waves," *IEEE J. Lightw. Technol.*, Vol. 26, No. 15, 2409–2423, Aug. 2008.
19. Huang, Y., N. Khiabani, D. Li, and Y. Shen, "Terahertz photoconductive antenna efficiency," *Int. Workshop on Antenna Tech.*, 152–156, Hong Kong, Mar. 2011.
20. Tanoto, H., J. H. Teng, Q. Y. Wu, M. Sun, Z. N. Chen, S. A. Maier, B. Wang, C. C. Chum, G. Y. Si, A. J. Danner, and S. J. Chua, "Greatly enhanced continuous-wave terahertz emission by nano-electrodes in a photoconductive photomixer,"

Nature Photon., Vol. 6, 121–126, Feb. 2012.

21. Balanis, C. A., *Antenna Theory: Analysis and Design*, 60–61, Wiley, New York, 1997.
22. Nguyen, T. K., H. Han, and I. Park, "Numerical study of a full-wavelength dipole antenna on a GaAs membrane structure at terahertz frequency," *J. Infrared Milli. Terahz Waves*, Vol. 32, No. 5, 763–777, 2011.
23. Saeedkia, D., R. R. Mansour, and S. Safavi-Naeini, "A submilliwatt terahertz high-temperature superconductive photomixer array source: Analysis and design," *IEEE Trans. on Appl. Superconductivity*, Vol. 15, No. 3, 3868–3873, Sep. 2005.
24. Rutledge D. B. and M. S. Muha, "Imaging antenna arrays," *IEEE Trans. Antennas Propagat.*, Vol. 30, No. 4, 535–540, Jul. 1982.
25. Nguyen, T. K., H. Han, and I. Park, "Full-wavelength dipole antenna on a hybrid GaAs membrane and Si lens for a terahertz photomixer," *J. Infrared Milli. Terahz Waves*, Vol. 33, 333–347, 2012.
26. CST Microwave Studio, CST GmbH, 2011, http://www.cst.com.
27. Alexopoulos, N. G., P. B. Katehi, and D. B. Rutledge, "Substrate optimization for integrated circuit antennas," *IEEE Trans. Microw. Theory Tech.*, Vol. 31, No. 7, 550–557, Jul. 1983.